Title: Early life regulatory T cells modulate PPARγ-dependent skin pigmentation.

Authors: Inchul Cho[1,2], Jessie Z. Xu[1,2], Shahnawaz Ali[1], Niwa H. Ali[1,2] *

Affiliations:

[1]Centre for Gene Therapy and Regenerative Medicine, King's College London, United Kingdom.

[2]Peter Gorer Department of Immunobiology, King's College London, United Kingdom.

*Corresponding author. Email: niwa.ali@kcl.ac.uk

Abstract: In the adult mouse skin, regulatory T cells (Tregs) control stem cell activation. However, whether Tregs are similarly important during stem cell-driven events, such as postnatal development, is unknown. Here, we reveal that during a transient period of postnatal development, neonatal Tregs are critical for PPARγ signalling in the skin, which is in turn necessary for the function of melanocyte stem cells, which produce skin pigmentation. Flow cytometry and immunofluorescence reveal Tregs in neonatal skin by postnatal day 3. These Tregs localise near hair follicles, and express 1.5-8-fold higher levels of activation markers CD25, CD27, CTLA4 and ICOS than their counterparts in the lymph node. Depletion of Tregs on postnatal day 6 (P6) and P8 disrupted skin pigmentation on P28. Transcriptomic analysis of the whole skin on P9 revealed immediate decreases in melanocyte stem cell markers and perturbation of PPARγ target genes in the hair follicles upon Treg depletion. In support of this observation, PPARγ antagonist T0070907 hinders pigmentation *in vivo*, while PPARγ agonist, GW1929, restores pigmentation in Treg-depleted mice. Therefore, Tregs sustain PPARγ signalling activity to regulate skin pigmentation. Finally, scRNA-seq analysis of vitiligo patients' skin reveals diminished PPARγ target genes in lesional keratinocytes. Similarly, scRNA-seq of Treg-sufficient and Treg-depleted mouse skin on day 9 uncovers reduced PPARγ pathway activity in HF keratinocytes. Overall, neonatal Tregs are key to sustaining skin PPARγ signaling, which is vital for melanocyte stem cell function and pigmentation.

One Sentence Summary: PPARγ pathway functions downstream of neonatal Tregs to regulate melanocyte stem cell function.

Main Text:

INTRODUCTION

Immune cells regulate stem cell differentiation and function both during homeostasis and injury (*1–3*). A central regulator of immune cells is the $CD4^+$ FoxP3+ regulatory T cells (Tregs), which are an immunosuppressive subset of T cells. In the skin, the Tregs are located in the vicinity of hair follicles (HF) (*1*, *4–6*). The HFs harbor distinct populations of stem cells, including HF stem cells (HFSCs) and melanocyte stem cells (MeSCs), governing hair shaft production and skin pigmentation, respectively. A Treg lineage-specific deletion of the Notch ligand, Jagged1, inhibits HFSC proliferation (*1*), revealing a stem cell regulatory function of Tregs that do not rely on its canonical immunosuppressive function.

Stem cell activity and immunity are both shaped during early life, which is an important phase of development. While functional differences between neonatal Tregs and adult Tregs have been noted (*7*), our understanding of neonatal skin Treg function is primarily limited to their role in

establishing tolerance towards commensal microbiota and suppressing type 2 immunity (*8*, *9*). The existence of a Treg-stem cell axis in neonates and its relevance to the homeostatic development and function of the skin remain largely unexplored.

In this study, we present a novel finding that neonatal Tregs define the functional capacity of MeSCs during a specific time window between postnatal day 6 (P6) and P8. Depletion of Tregs during this critical period, but not later, results in defective melanocyte function, as evidenced by transcriptomic and histological analyses. Notably, the transcriptomic changes in melanocyte function precede the inflammatory responses following Treg depletion, suggesting that Tregs may regulate MeSCs independently of secondary mediators such as $CD4^+$ $FoxP3^-$ effector T cells or $CD8^+$ cytotoxic T cells.

Furthermore, we observed an immediate downregulation of transcripts associated with the PPAR pathway (Peroxisome proliferator-activated receptor) in response to early Treg depletion. To investigate this pathway further, we intraperitoneally administered a small molecule PPARγ antagonist, T0070907, which disrupted skin pigmentation *in vivo*. Conversely, an administration of the PPARγ agonist, GW1929, was sufficient to restore melanogenic activity of MeSCs in the early Treg-depleted skin. Additionally, we observed changes in PPARγ signalling activity through development of the human skin, and between pigment-deficient states, such as vitiligo. These findings corroborate our mouse studies and further support the requirement of the PPARγ pathway for melanogenic activity. Taken together, our findings provide novel insights into the function of neonatal Tregs, which are essential for the establishment of functional stem cells during postnatal development of the skin.

RESULTS

Skin Tregs accumulate within the first 2 weeks after birth

Peripheral tissues recruit Tregs from the thymus on postnatal day 3 (P3) (*10*). Accumulation of skin Tregs is largely driven by commensal microbiota (*11*). Given potential variability of microbiome between animal housing facilities, we first characterised Treg abundance and phenotypic markers in the neonatal skin and skin-draining lymph node (SDLN) of *Foxp3-DTR* transgenic mice by flow cytometry (**Supplementary figure 1A-D**). Flow cytometric profiling revealed the presence of Tregs at low numbers on P3 (**Figure 1A-B**). The number and percentage of Tregs steadily increased and peaked during the second week after birth, which is consistent with previous study reporting a peak of Treg numbers on P13 (**Figure 1A-B**) (*9*). Of note, Treg percentages on P9 and P12 were comparable to that found in adult skin on P49 (**Figure 1A**). This observation corroborates a recent study reporting that skin Treg percentage in neonates is similar to that found in adults (*12*). By contrast, the percentage of $FoxP3^+$ Tregs remained steady in the SDLN. A peak abundance of other skin T cells was not sustained through to adulthood (**Supplementary figure 2A-F**). Approximately 60% of skin Tregs were $Ki67^+$ proliferating cells on P5, suggesting both local expansion and seeding from the thymus and SDLN contribute to Treg accumulation in the skin (*11*) (**Supplementary figure 2C, 2F**).

Given the drastic changes in the skin Treg numbers during neonatal stages, we assessed the expression of activation markers (CD25, CD27, ICOS and CTLA4) on Tregs to as a proxy of their function. The MFI of Treg activation markers fluctuated by 4 to 6-fold in the skin, whereas Tregs in the SDLN expressed markedly lower levels of these markers, except CD27, compared

to their skin-resident counterparts (**Figure 1C-D**). These observations led us to hypothesise that Tregs may play an important role during postnatal skin development. We therefore depleted Tregs in neonatal *Foxp3-DTR* mice on P6, P8, P10 and P12 (ΔTreg). Subsequently, we assessed hallmarks of stem cell activity (skin pigmentation, and stem cell proliferation) on P28, a period of stem cell activation in the mouse skin (*13*). We observed a significant defect in pigmentation in ΔTreg group on P28 indicating that Tregs regulate the melanogenic function of MeSCs in the HFs (**Supplementary figure 3A-C**). However, these ΔTreg mice gain significantly less weight over the period of the experiment (**Supplementary figure 3D**), likely due to an immediate inflammatory response that persists until P28 despite an increased abundance of re-populating Tregs in ΔTreg skin (**Supplementary figure 3E-I**). Overall, depletion of neonatal Tregs lead defective pigmentation, but mice succumb to a systemic inflammation. The same Treg depletion regimen in adult mice do not cause an inflammation (*1*). Our observation therefore further supports the idea that neonatal and adult Tregs are functionally distinct (*7*).

Early, and not late, neonatal Tregs are required for skin pigmentation

A 4-dose depletion of Tregs resulted in weight loss accompanied by an immediate inflammatory response on P13, persisting until P28 (**Supplementary figure 3E-I**). To refine the depletion regimen, we implemented a 2-dose regimen that effectively depleted both early skin Tregs (ΔeTreg) by administering DT on P6 and P8 and late skin Tregs on P10 and P12 (ΔlTreg) (**Supplementary figure 4A-B**). Fontana & Masson (F&M) staining revealed a significant reduction in skin pigmentation in the ΔeTreg group compared to littermate controls injected with PBS (**Figure 2A-C**). Conversely, the ΔlTreg group did not show a statistically significant reduction in pigmentation. Importantly, weight gain of ΔeTreg groups from P6 to P49 was comparable to control groups (**Supplementary figure 4C**). Therefore, an early 2-dose depletion regimen, but not late, impairs skin pigmentation without compromising fitness of the animals.

Next, we performed flow cytometry to test the hypothesis that the observed defective skin pigmentation is linked to a disruption of the stem cell maintenance or activity. Profiling of MeSCs and HFSCs showed that both their numbers and percentage Ki67 expression remain comparable between control and ΔeTreg groups on P28 (**Figure 2F-G**). Therefore, SC maintenance is unaffected in the absence of neonatal Tregs.

Given the important role of T cells in skin pigmentation (*14*), we assessed whether skin T cell numbers are affected in ΔeTreg skin. Indeed, the skin T cell pool expands, but maintains homeostatic level of proliferation, Teff:Treg ratios, and CD8:Treg cell ratios. (**Figure 2H-J**). Additionally, Teff numbers decreased in ΔeTreg skin on P9, whilst other T cell numbers and their proliferative statuses were unaffected (**Figure 2K-L**). Nonetheless, we observed an increased IFNγ production by $CD8^+$ T cells in the skin on P9 following Treg depletion (**Supplementary figure 5A-E**), and elevated levels of IFNγ and TNFα in the SDLN (**Supplementary figure 5F-I**). However, a depletion of $CD8^+$ T cells in ΔeTreg mice did not rescue skin pigmentation. Altogether, our results suggest that T cells are dispensable for skin pigmentation downstream of Tregs.

Melanocytes and PPARγ pathway are disrupted immediately following Treg depletion

To investigate the mechanisms underlying early Treg-pigmentation axis, we performed whole skin bulk RNA-seq analysis using skin tissues from the control, ΔeTreg, ΔlTreg, and ΔTreg groups on the day following the last treatment (P9 or P13, depending on the treatment regimen) (**Figure 3A**). The aim of this experiment was to identify transcriptomic changes that contribute

to defective pigmentation on P28. We conducted a pathway enrichment analysis using differentially expressed genes ($p<0.05$) with ShinyGO (*15*). Transcriptomic defects related to melanocytes and interferon-β responses were evident in the ΔeTreg group on P9 compared to age-matched controls (**Figure 3B**). Conversely, the ΔlTreg group displayed changes primarily associated with cell development and morphogenesis (**Figure 3C**). These observations suggest that melanocytes are one of the primary cell types that are affected upon early Treg depletion. This notion is further substantiated by the downregulation of key melanocyte markers (*Tyr*, *Tyrp1*, *Dct*, *Slc45a2*, *Oca2*, *Slc24a5*) specifically in the ΔeTreg and ΔTreg groups, but not in the ΔlTreg group, compared to age-matched controls (**Figure 3D**). Quantification of CD117+ MeSCs *in situ* demonstrated that these transcriptomic changes were not attributed to a quantitative reduction in MeSC numbers (**Figure 3E-F**). Rather, it is likely that MeSCs become less functional in the ΔeTreg group due to the downregulation of transcripts associated with melanin synthesis, such as *Tyr* and *Oca2*.

To identify the signaling pathways responsible for pigmentation downstream of neonatal Tregs, we employed specific inclusion criteria based on the observation that pigmentation fails to develop in the ΔeTreg and ΔTreg groups. We selected genes that met the following criteria: 1) Not differentially expressed between the ΔeTreg and ΔTreg groups, 2) Differentially expressed between the ΔlTreg and ΔTreg groups, and 3) Differentially expressed between the control and ΔTreg groups (**Figure 3G**). We identified 195 genes that fulfilled these criteria. Pathway enrichment analysis revealed a disruption in the PPAR (peroxisome proliferator-activated receptor) pathway (**Figure 3H**). To validate the changes in the PPAR pathway, we performed RNAscope analysis to quantify the expression of PPARγ target genes, *Fabp7* and *Adipoq*. *In situ* quantification of transcripts specifically in the HFs showed a significant reduction of *Fabp7* and *Adipoq* expression upon depletion of early Tregs on P9 (**Figure 3I-L**). Overall, our findings confirm the presence of a transient window for the Treg-MeSC axis, during which depleting Tregs leads to disruption of PPARγ signalling pathway. Notably, the transcriptomic changes occur immediately following Treg depletion.

PPARγ pathway is necessary and sufficient for pigmentation

We next sought to determine signalling pathways are responsible for pigmentation defect downstream of Tregs. In ΔeTreg skin, changes in interferon-β response and PPAR signalling pathway occur (**Figures 3B**). These candidates have all previously been associated with melanocyte function (*16*, *17*). Skin pigmentation was not re-instated upon Ifnar-blocking antibodies ruling out interferon-β responses as candidate pathways (**Supplementary figure 6B**).

Amongst three isoforms of PPAR (PPARα, β and γ), only the PPARγ is expressed at higher levels in neonatal skin than in adult skin (*18*). Therefore, we set out to assess whether neonatal PPARγ signalling is necessary for skin pigmentation. Firstly, we intraperitoneally administered neonatal mice with a highly specific PPARγ antagonist, T0070907 on P6 and P8 (**Figure 4A**). As expected, T0070907 treatment impaired skin pigmentation (**Figure 4B-E**, **Supplementary figure 6C**). Defective skin pigmentation was accompanied by a reduction in the number, but not proliferation, of MeSCs (**Figure 4F-G**). As such, neonatal PPARγ signalling may be crucial for MeSC maintenance.

To validate whether PPARγ functions downstream of Tregs, we administered a highly specific PPARγ agonist, GW1929, to Treg-depleted animals on P6 and P8 (**Figure 4H**). PPARγ agonisation restored skin pigmentation in Treg-depleted mice (**Figure 4I-L**, **Supplementary**

figure 6D). However, MeSC numbers and proliferation were unaffected by PPARγ agonisation (**Figure 4M-N**). Therefore, GW1929 may restore pigmentation via qualitative increase in the melanogenic potential of MeSCs. Lastly, the observed PPARγ-dependent changes in skin pigmentation were not significant alterations in T cell numbers on P28 (**Supplementary figure 7A-H**). Therefore, it seems likely that Treg-PPARγ axis functions independently of T cells. Overall, our findings suggest a possibility that Tregs may regulate melanocytes independently of its canonical immunosuppressive function by controlling PPARγ signalling activity in the skin.

Human melanocyte development and pigmentary disorders are associated with PPARγ pathway

Vitiligo, a pigmentary disorder characterised by defective skin pigmentation, is closely associated with small nucleotide polymorphisms (SNPs) in Treg super-enhancer regions (*19*). Additionally, Treg seeding of the human skin is observed as early as gestational week (GW) 18 (*18*, *20*). This period of Treg infiltration co-incides with the human HF development, which involves the migration of melanoblasts to the HF (*21*). Given these associations between Tregs and human pigmentation, we sought to address whether changes in PPARγ signalling activity is associated with vitiligo and development of melanocytes. To address this, we analysed single-cell transcriptomic data of fetal (9.5-18 GW), neonatal (0 years), and adult (24-81 years) melanocytes, and skin tissues from healthy donors and vitiligo patients (*22*, *23*).

Namely, we examined whether PPARγ target gene expression changes during development. Chi-squared analysis revealed a marked enrichment of adult and neonatal melanocytes for cluster 0, while fetal melanocytes were enriched for cluster 2 (**Figure 5A-B**). Differential expression analysis identified elevated expression of multiple PPARγ target genes in cluster 0 (**Figure 5C**) (*24*). The expansion of cluster 0 post-18 GW temporally co-incides with Treg seeding, and therefore supports our findings that Tregs are crucial for PPARγ signalling activity. Finally, we analysed scRNA-seq data of human skin samples from healthy donors and vitiligo patients (*23*). We scored for PPARγ target gene expression using experimentally validated gene sets (*25*), and identified a population of keratinocytes with a marked PPARγ score (**Figure 5D**). The PPARγ score was reduced (p=0.08) in diseased keratinocytes relative to those found in the healthy skin (**Figure 5E**). Collectively, our data suggests that neonatal Tregs may regulate PPARγ signalling activity in the human skin, and that PPARγ signalling is disrupted in Treg-associated conditions such as vitiligo.

Keratinocyte-intrinsic PPARγ signalling activity relies on the presence of Tregs

To further elucidate the cellular mechanisms of Treg-PPARγ axis, we performed scRNA-seq of control and ΔeTreg skin on P9. Firstly, we quantified $CD45^+$ immune cell subsets to confirm whether inflammatory accumulation of immune cells, including myeloid cells, occur. In support with our flow cytometric profiling on P9, we observed minimal change in T cell numbers in ΔeTreg skin (**Figure 6A-B**). As such, the skin is minimally inflamed on P9 following Treg depletion, concordant with our prior findings (**Supplementary figure 4A-E**). We also analysed $CD45^-$ immune cells and identified melanocytes, and keratinocytes, and other structural cells such as fibroblasts and vascular endothelial cells. The abundance of these cells were also minimally affected in ΔeTreg skin (**Figure 6C-D**).

Next, we performed a differential expression analysis to ascertain the magnitude transcriptomic changes induced in the ΔeTreg skin. The transcriptome of hair follicles (Ana and HF) were most

affected, followed by innate lymphoid cells and macrophages (**Figure 6E**). This observation strongly suggests that the HFs, and not immune cells, are the primary targets of neonatal Tregs.

Finally, we assessed for changes in PPARγ activity by scoring for PPARγ target gene expression (**Figure 6F-I)**. Neutrophils, macrophages, and melanocytes scored highly for PPARγ activity, which is in line with the known role for PPARγ in these cells (*26*, *27*). However, PPARγ score in these cells were unaffected in ΔeTreg skin. Instead, PPARγ score was reduced in HF keratinocytes (**Figure 6I**).

Overall, scRNA-seq analysis revealed that the HF transcriptome, and their PPARγ activity, are affected in ΔeTreg skin. As such, neonatal Tregs may regulate MeSC function by sustaining PPARγ signalling in HF keratinocytes.

DISCUSSION

In this study, we made the discovery that neonatal Tregs play a crucial role in the development of skin pigmentation. We observed rapid fluctuations in the expression of Treg phenotypic markers during early neonatal stages, suggesting a temporal dynamic in Treg function. Indeed, depletion of early Tregs led to impaired pigmentation, while depletion of late Tregs did not. Furthermore, depletion of neonatal Tregs on P8 and P15 disrupts tissue architecture (*8*). Remarkably, transcriptomic changes related to melanocyte function and the PPARγ pathway occurred immediately after early Treg depletion, occurring before any signs of an inflammatory response. An agonisation of neonatal PPARγ signalling re-instated skin pigmentation, strongly supporting its role downstream of Tregs.

In addition to its immunomodulatory functions, the PPARγ pathway is known to be involved in the accumulation and adaptation of Tregs within adipose tissue microenvironments, such as the dermal white adipose tissue underneath the dermis (*28*). However, skin T cell numbers were unaffected by a transient antagonisation of neonatal PPARγ activity. This suggests that the Treg-melanocyte axis operates independently of immune cells. Moreover, skin pigmentation was not restored in ΔeTreg mice upon depletion of $CD8^+$ T cells or a blockade of interferon-β response. Together, these observations support the idea that immune cells are unlikely to be involved in the regulation of skin pigmentation by Tregs.

Finally, our study suggests that Tregs regulate PPARγ activity within the HF epithelium (**Figure 3I-L, 6I**). The transcriptome of HFs is more affected than any other cell types immediately upon depletion of neonatal Tregs (**Figure 6E**). Together, these observations suggest that the primary target of neonatal Tregs are the HF epithelial cells, instead of T cells. This notion is further corroborated by our finding that Tregs reside in closer proximity to MeSCs than $CD8^+$ T cells or Teffs (**Supplementary figure 8A-C**). In the developing human skin, changes in PPARγ activity co-incides with Treg seeding (*29*). Moreover, PPARγ activity decreases in skin affected by vitiligo (**Figure 5E**). As such, Tregs are likely to contribute to PPARγ signalling in the human skin.

A major limitation of our study is the use of PPARγ modulators, instead of transgenics. Melanocyte number decreases in T0070907-treated mice, but not in ΔeTreg mice (**Figure 2F, 4F**). Therefore, it is possible that different mechanisms lead to pigmentation defect in ΔeTreg and T0070907-treated groups. This discrepancy may be explained our observation that melanocytes are most dependent on PPARγ signalling activity in the developing mouse skin, and therefore most vulnerable to PPARγ antagonists (**Figure 6G**).

Overall, our investigation provided new insights into the elusive function of neonatal Tregs in the skin. Our studies in mice point towards temporal dynamic in Treg function, whereby early neonatal Tregs regulate melanocytes, but not late neonatal Tregs. GWAS studies showed that Tregs malfunction is associated with vitiligo (*30*). But, whether Treg malfunction during early life contributes to its pathogenesis was unknown. Our studies suggest a possibility that disruption of Treg function during development may lead to an impairment of a Treg-PPARγ signalling axis that perturbs melanogenic functions of MeSCs.

MATERIALS AND METHODS

Mouse studies

All animal experiments were subject to local ethical approval and performed under the terms of a UK government Home Office licence (PP6051479). All mice were outbred on a C57BL/6J background. Both male and female mice were used. B6.129(Cg)-Foxp3$^{tm3(DTR/GFP)}$Ayr/J (Foxp3-DTR) mice were purchased from Jackson laboratories. For Treg depletion, *Foxp3-DTR* mice intraperitoneally received 30 ng/g of DT on P6 and P8. PPARγ antagonisation was performed by intraperitoneal administration of 2.5 µg/g of T0070907 on P6 and P8. Rescue studies were performed by intraperitoneal administration of 30 ng/g of DT and 20 µg/g of GW1929 on P6 and P8. CD8^{+} T cells were depleted by intraperitoneal administration of 100 µg of α-CD8 depleting antibody (BioXcell) on P6, P8, P15 and on P22. Interferon-β responses were blocked by intraperitoneal administration of α-Ifnar blocking antibody (Biolegend) on P6 and P8. Pre-weanlings were sacrificed by overdose of pentobarbital. Post-weanlings were sacrificed by CO2 asphyxiation followed by severing a major blood vessel. All efforts were made to minimise suffering for mice.

Tissue digestion

Single-cell suspensions of full-thickness skin for flow cytometry was performed as previously described (*1*). Isolation of cells from axillary, brachial and inguinal lymph nodes for flow cytometry was performed by mashing tissue over 70 µm sterile filters. To prepare dorsal skin cell suspension, shaved mouse skin was de-fatted, minced finely with scissors, and re-suspended in a 3 ml of C10 (RPMI-1640 with L-glutamine with 10% heat-inactivated FBS, 1% penicillin-streptomycin, 1 mM Sodium pyruvate, 1% Hepes, 1x Non-essential amino acid and 60 µM β-mercaptoethanol) supplemented with 2mg/ml collagenase XI, 0.5mg/ml hyaluronidase and 0.1mg/ml DNase in a 50 ml conical. The mixture was digested in a shaking incubator at 37°C at 255 rpm for 45 mins. After a vigorous shaking, the digested mixture was passed through a sterile 100 µm filter fitted onto a 50 ml conical. After pelleting, the filtrate was then filtered once more through a 40 µm strainer fitted onto a new 50 ml conical. Finally, the cells were pelleted once more and re-suspended in 1 ml of C10. Epidermal cell suspensions were prepared by scraping the dermis away with forceps and incubating the layer of epidermis on 3 mL of 0.5% Trypsin-EDTA (ThermoFisher) at 37˚C for 1 hour. Epidermal cells were isolated by scraping the trypsinised epidermis on a petri dish containing 4 ml of C10 media. The mixture of cell suspension and scraped skin was filtered through a 70 µm strainer fitted onto a 50 ml conical. Finally, the cells were pelleted and re-suspended in C10. After cell count using nucleocounter (Chememoetec), cells were plated on nunc round bottom 96-well plates (Thermofisher) for staining.

Flow cytometry

Following isolation from the tissue, cells were labeled stained in PBS for 20 mins at 4°C with a live dead marker (Zombie UV^{TM}, Biolegend). Surface staining was performed in brilliant stain buffer (BD Biosciences) for 20 mins at 4˚C. For intracellular staining, cells were fixed and permeabilized using reagents and protocol from the Foxp3 staining buffer kit (eBioscience). Fluorophore-conjugated antibodies specific for mouse cell surface antigens and intracellular transcription factors were purchased from eBioscience, BD Biosciences or Biolegend as detailed in the Supplementary Table 1. All samples were run on Fortessa LSRII (BD Biosciences) at the KCL BRC Flow Cytometry Core. Experiments were standardised using SPHERO Rainbow calibration particle, 8 peaks (BD Biosciences, 559123). For compensation, UltraComp eBeads (Thermo Fisher, 01-2222-42) were stained for each surface and intracellular antibody following the same procedure as cell staining. ArC Amine Reactive Compensation Bead Kit (Thermo Fisher, A10346) were used for Zombie UV^{TM} stain. All gating and data analysis were performed using FlowJo v10, while statistics were calculated using GraphPad Prism 9. Strict dead cell and doublet cell exclusion criteria were included for all immune cell analysis, followed by pre-gating for all hematopoietic cells as CD45^{+}. All immune cells were pre-gated as Zombie UV^{-} CD45^{+} cells. CD3^{-} lymphoid/myeloid cells were gated TCR$^{\gamma\delta-}$CD3^{-} double negative cells. Other lymphoids were gated as TCRγδ^{+}CD3^{+} dermal γδ T cells (dGDTCs), TCRγδ^{hi}CD3^{hi} dendritic epidermal T cells (DETCs), TCDγδ^{-}CD3^{+}CD8^{+} T cells (CD8), TCRγδ^{-}CD3^{+}CD4^{+}Foxp3^{-} T effector cells (Teff), and TCRγδ^{-}CD3^{+}CD4^{+}Foxp3^{+} regulatory T cells (Tregs).

T cell stimulation

PMA/Ionomycin cocktail (Tonbo Biosciences) was diluted to 1x concentration in C10. Heat-inactivated FBS must be used to make C10 for cell stimulation. 6 to 8 million live cells were re-suspended in 200 µl of 1x PMA/Ionomycin cocktail and plated on a round-bottom 96-well plate (Thermofisher Scientific). Re-suspended cells were incubated at 37˚C for 4 hours. Stimulated cells were centrifuged at 1800 rpm for 4 minutes at 4˚C. Cell pellets were washed by topping up with 200 µl of FACS buffer and centrifugation at 1800 rpm for 4 minutes at 4˚C. Washed cells were stained as follows: live/dead staining for 20 minutes on ice; surface staining overnight at 4˚C; and intracellular staining overnight at 4˚C.

Histology and microscopy

Loose fatty tissues were removed from shaved dorsal skin with a pair of forceps. The skin was fixed in 10% neutral buffered formalin (Fisher Scientific) overnight at 4˚C. On the following day, fixed tissues were washed twice in PBS for 5 mins each on a rocking platform. Following wash, skin tissues were either stored in 70% EtOH at 4˚C to later be embedded in paraffin.

Immunofluorescence and tissue microarray

Immunofluorescence labelling was performed using tissue microarrays generated using a manual tissue arrayer (Beechers Instruments). Individual tissue cores (4 mm diameter) were extracted from FFPE skin tissue blocks and moved to a recipient block using a Beechers MTA1 manual tissue arrayer (Beechers Instruments). Multiplex staining was performed using the following antibodies anti-FoxP3 (14-5773-82, Thermofisher), anti-DCT (ab74073, Abcam), and anti-CD117 (AF1356, RnD systems). Immunohistochemical experiments were conducted using Bond Max automated staining system (Leica, UK). Each antibody was optimized for pH and concentration dependence, antigen retrieval and temperature parameters. RNAscope was performed as per manufacturer's protocol. Confocal microscopy was performed with a Leica SP8 confocal microscope using a ×20 objective. Fontana & Masson staining was performed as

per manufacturer's protocol (Abcam). F&M slides were imaged using a Nanozoomer (Hamamatsu photonics) with a ×40 objective.

In situ transcript quantification

RNA-scope slides were analysed using QuPath (*31*). Cells were detected using the DAPI channel. Transcript counts per cell was quantified using built-in subcellular spot detection function.

Pigmentation index

Pigmentation index was calculated from F&M images as follows. Images were converted to 16-bit using Fiji. Otsu method thresholding was performed to filter for black pixels corresponding to melanin. Area of melanin was measured and normalised to the length of the skin.

Whole skin RNA-seq

4 mm biopsy of skin samples were stored in RNAlater (Sigma) at -20˚C. Skin samples were homogenised with Kinematica™ Polytron™ handheld PT1200E homogeniser (Fisher Scientific) using a 1200E probe (Fisher Scientific). The RNA was extracted using the mirVana™ miRNA Isolation kit (Invitrogen) by following the manufacturer's protocol. Prior to start of digestion, and between samples, the probe was sequentially washed in 1% SDS, 100% ethanol and dH2O to avoid cross-contamination. Samples were maintained on ice at all times. Extracted RNA was stored at -20˚C. Concentration of the RNA was determined using Qubit™ Broad Range assay kit (Invitrogen). Quality of the RNA was checked using Bioanalyzer (Agilent Technologies) at the King's Genomics Centre. Only samples with RNA integrity score greater than 7.0 were taken further for downstream applications. 2 µg of total RNA per samples were used for RNA-seq. 150 bp paired-end Sequencing was performed on the NovaSeq platform (Illumina) at Genewiz. Sequenced reads were trimmed using Trimmomatic v.0.36. Trimmed reads were mapped to the Mus musculus GRCm38 reference genome using the STAR aligner v.2.5.2b to produce BAM files. Unique gene counts were calculated using featureCounts function from the Subread package v.1.5.2. Only reads that fell within exon regions were counted to generate the gene hit counts table. Differential expression analysis was performed using DESeq2. Wald test was used to generate p-values and log2 fold changes.

Pathway analysis

An enrichment analysis was performed to extract biological information from the list of pigmentation-associated genes. The enrichment analysis was performed using a web-based platform, ShinyGO (136). A false discovery rate cut-off of 0.3 was used for the list of pigmentation-associated genes. All other pathway analysis was performed with a false discovery rate cut-off of 0.05.

Mouse skin scRNA-seq

Skin $CD45^+$ and $CD45^-$ cells were FACS-sorted into RPMI-1640 supplemented with 40% heat-inactivated FBS and 40 U/ml of RiboLock RNase inhibitor (Thermofisher). The cells numbers were counted and mixed at 2:1 ratio ($CD45^+$:$CD45^-$). The mixed cells were used for cDNA library generation using the 10X Genomics Chromium Sinlge cell 3' kit by the Genomics Centre at the Blizard Institute. Prepared libraries were sequenced using the NovaSeq 6000 S4. Raw sequencing data were processed using the 10X Genomics *CellRanger* package.

Human skin scRNA-seq

Human neonatal and adult melanocyte scRNA-seq data is available in the Gene Expression Omnibus (GEO) database repository under accession number GSE151091. Human healthy and vitiligo skin scRNA-seq data is available in the Genome Sequence Archive (GSA) with accession number PRJCA006797. Analysis was performed using Seurat package in the R programming environment.

Statistical analysis

Statistical analysis was performed using GraphPad Prism 8.0 (GraphPad Inc.). Unpaired t-test, paired t-test or one way ANOVA was performed as indicated in figure legends to calculate p values. Statistical significance was inferred if p value was less than 0.05 (*), 0.01 (**), 0.001 (***), or 0.0001 (****). P values greater than 0.05 was identified as not statistically significant.

Supplementary Materials

Supplementary figure 1. Flow cytometric gating strategy for analysis.

Supplementary figure 2. Flow cytometric characterisation of T cell numbers and proliferation.

Supplementary figure 3. Four-dose DT regimen causes weight loss, inflammation, and pigment defect.

Supplementary figure 4. Transient DT injection is sufficient for skin Treg depletion.

Supplementary figure 5. Early Treg depletion causes inflammatory response in the skin and SDLN.

Supplementary figure 6. Modulation of skin pigmentation.

Supplementary figure 7. Modulation of neonatal PPARγ signalling does not affect skin-resident immune cell numbers or proliferation.

Supplementary figure 8. Skin Tregs reside proximally to melanocyte stem cells, and not T cells.

References

1. N. Ali, B. Zirak, R. S. Rodriguez, M. L. Pauli, H. A. Truong, K. Lai, R. Ahn, K. Corbin, M. M. Lowe, T. C. Scharschmidt, K. Taravati, M. R. Tan, R. R. Ricardo-Gonzalez, A. Nosbaum, M. Bertolini, W. Liao, F. O. Nestle, R. Paus, G. Cotsarelis, A. K. Abbas, M. D. Rosenblum, Regulatory T Cells in Skin Facilitate Epithelial Stem Cell Differentiation. *Cell* (2017), doi:10.1016/j.cell.2017.05.002.

2. M. Biton, A. L. Haber, N. Rogel, G. Burgin, S. Beyaz, A. Schnell, O. Ashenberg, C. W. Su, C. Smillie, K. Shekhar, Z. Chen, C. Wu, J. Ordovas-Montanes, D. Alvarez, R. H. Herbst, M. Zhang, I. Tirosh, D. Dionne, L. T. Nguyen, M. E. Xifaras, A. K. Shalek, U. H. von Andrian, D. B. Graham, O. Rozenblatt-Rosen, H. N. Shi, V. Kuchroo, O. H. Yilmaz, A. Regev, R. J. Xavier, T Helper Cell Cytokines Modulate Intestinal Stem Cell Renewal and Differentiation. *Cell* (2018), doi:10.1016/j.cell.2018.10.008.

3. F. Gerbe, E. Sidot, D. J. Smyth, M. Ohmoto, I. Matsumoto, V. Dardalhon, P. Cesses, L. Garnier, M. Pouzolles, B. Brulin, M. Bruschi, Y. Harcus, V. S. Zimmermann, N. Taylor,

R. M. Maizels, P. Jay, Intestinal epithelial tuft cells initiate type 2 mucosal immunity to helminth parasites. *Nature* (2016), doi:10.1038/nature16527.

4. I. K. Gratz, H.-A. Truong, S. H.-Y. Yang, M. M. Maurano, K. Lee, A. K. Abbas, M. D. Rosenblum, Cutting Edge: Memory Regulatory T Cells Require IL-7 and Not IL-2 for Their Maintenance in Peripheral Tissues. *J. Immunol.* (2013), doi:10.4049/jimmunol.1300212.

5. R. S. Rodriguez, M. L. Pauli, I. M. Neuhaus, S. S. Yu, S. T. Arron, H. W. Harris, S. H. Y. Yang, B. A. Anthony, F. M. Sverdrup, E. Krow-Lucal, T. C. MacKenzie, D. S. Johnson, E. H. Meyer, A. Löhr, A. Hsu, J. Koo, W. Liao, R. Gupta, M. G. Debbaneh, D. Butler, M. Huynh, E. C. Levin, A. Leon, W. Y. Hoffman, M. H. McGrath, M. D. Alvarado, C. H. Ludwig, H. A. Truong, M. M. Maurano, I. K. Gratz, A. K. Abbas, M. D. Rosenblum, Memory regulatory T cells reside in human skin. *J. Clin. Invest.* (2014), doi:10.1172/JCI72932.

6. Z. Chow, S. N. Mueller, J. A. Deane, M. J. Hickey, Dermal Regulatory T Cells Display Distinct Migratory Behavior That Is Modulated during Adaptive and Innate Inflammation. *J. Immunol.* (2013), doi:10.4049/jimmunol.1203205.

7. S. Yang, N. Fujikado, D. Kolodin, C. Benoist, D. Mathis, Regulatory T cells generated early in life play a distinct role in maintaining self-tolerance. *Science (80-.).* (2015), doi:10.1126/science.aaa7017.

8. I. C. Boothby, M. J. Kinet, D. P. Boda, E. Y. Kwan, S. Clancy, J. N. Cohen, I. Habrylo, M. M. Lowe, M. Pauli, A. E. Yates, J. D. Chan, H. W. Harris, I. M. Neuhaus, T. H. McCalmont, A. B. Molofsky, M. D. Rosenblum, Early-life inflammation primes a T helper 2 cell–fibroblast niche in skin. *Nature* (2021), doi:10.1038/s41586-021-04044-7.

9. T. C. Scharschmidt, K. S. Vasquez, H. A. Truong, S. V. Gearty, M. L. Pauli, A. Nosbaum, I. K. Gratz, M. Otto, J. J. Moon, J. Liese, A. K. Abbas, M. A. Fischbach, M. D. Rosenblum, A Wave of Regulatory T Cells into Neonatal Skin Mediates Tolerance to Commensal Microbes. *Immunity* (2015), doi:10.1016/j.immuni.2015.10.016.

10. Y. Nishizuka, T. Sakakura, Thymus and reproduction: Sex-linked dysgenesia of the gonad after neonatal thymectomy in mice. *Science (80-.).* (1969), doi:10.1126/science.166.3906.753.

11. T. C. Scharschmidt, K. S. Vasquez, M. L. Pauli, E. G. Leitner, K. Chu, H. A. Truong, M. M. Lowe, R. Sanchez Rodriguez, N. Ali, Z. G. Laszik, J. L. Sonnenburg, S. E. Millar, M. D. Rosenblum, Commensal Microbes and Hair Follicle Morphogenesis Coordinately Drive Treg Migration into Neonatal Skin. *Cell Host Microbe* (2017), doi:10.1016/j.chom.2017.03.001.

12. P. Sivasami, C. Elkins, P. P. Diaz-Saldana, K. Goss, A. Peng, M. Hamersky IV, J. Bae, M. Xu, B. P. Pollack, E. M. Horwitz, C. D. Scharer, L. Seldin, C. Li, Obesity-induced dysregulation of skin-resident PPARγ^{+} Treg cells promotes IL-17A-mediated psoriatic inflammation. *Immunity*. **56**, 1844-1861.e6 (2023).

13. S. Müller-Röver, B. Handjiski, C. Van Der Veen, S. Eichmüller, K. Foitzik, I. A. McKay, K. S. Stenn, R. Paus, A comprehensive guide for the accurate classification of murine hair follicles in distinct hair cycle stages. *J. Invest. Dermatol.* (2001), , doi:10.1046/j.0022-

202X.2001.01377.x.

14. J. E. Harris, T. H. Harris, W. Weninger, E. J. Wherry, C. A. Hunter, L. A. Turka, A mouse model of vitiligo with focused epidermal depigmentation requires IFN-γ for autoreactive CD8+ T-cell accumulation in the skin. *J. Invest. Dermatol.* (2012), doi:10.1038/jid.2011.463.

15. S. X. Ge, D. Jung, D. Jung, R. Yao, ShinyGO: A graphical gene-set enrichment tool for animals and plants. *Bioinformatics* (2020), doi:10.1093/bioinformatics/btz931.

16. K. Krasagakis, C. Garbe, S. Krüger, C. E. Orfanos, Effects of interferons on cultured human melanocytes in vitro: Interferon-beta but not -alpha or -gamma inhibit proliferation and all interferons significantly modulate the cell phenotype. *J. Invest. Dermatol.* (1991), doi:10.1111/1523-1747.ep12480767.

17. J. S. Lee, Y. M. Choi, H. Y. Kang, PPAR-gamma agonist, ciglitazone, increases pigmentation and migration of human melanocytes. *Exp. Dermatol.* (2007), doi:10.1111/j.1600-0625.2006.00521.x.

18. L. Michalik, B. Desvergne, N. S. Tan, S. Basu-Modak, P. Escher, J. Rieusset, J. M. Peters, G. Kaya, F. J. Gonzalez, J. Zakany, D. Metzger, P. Chambon, D. Duboule, W. Wahli, Impaired skin wound healing in peroxisome proliferator-activated receptor (PPAR)α and PPARβ mutant mice. *J. Cell Biol.* (2001), doi:10.1083/jcb.200011148.

19. N. Ohkura, Y. Yasumizu, Y. Kitagawa, A. Tanaka, Y. Nakamura, D. Motooka, S. Nakamura, Y. Okada, S. Sakaguchi, Regulatory T Cell-Specific Epigenomic Region Variants Are a Key Determinant of Susceptibility to Common Autoimmune Diseases. *Immunity*. **52** (2020), doi:10.1016/J.IMMUNI.2020.04.006.

20. M. O. Dhariwala, D. Karthikeyan, K. S. Vasquez, S. Farhat, A. Weckel, K. Taravati, E. G. Leitner, S. Clancy, M. Pauli, M. L. Piper, J. N. Cohen, J. F. Ashouri, M. M. Lowe, M. D. Rosenblum, T. C. Scharschmidt, Developing Human Skin Contains Lymphocytes Demonstrating a Memory Signature. *Cell Reports Med.* **1** (2020), doi:10.1016/j.xcrm.2020.100132.

21. M. Cichorek, M. Wachulska, A. Stasiewicz, A. Tymińska, Skin melanocytes: Biology and development. *Postep. Dermatologii i Alergol.* (2013), doi:10.5114/pdia.2013.33376.

22. R. L. Belote, D. Le, A. Maynard, U. E. Lang, A. Sinclair, B. K. Lohman, V. Planells-Palop, L. Baskin, A. D. Tward, S. Darmanis, R. L. Judson-Torres, Human melanocyte development and melanoma dedifferentiation at single-cell resolution. *Nat. Cell Biol.* (2021), doi:10.1038/s41556-021-00740-8.

23. Z. Xu, D. Chen, Y. Hu, K. Jiang, H. Huang, Y. Du, W. Wu, J. Wang, J. Sui, W. Wang, L. Zhang, S. Li, C. Li, Y. Yang, J. Chang, T. Chen, Anatomically distinct fibroblast subsets determine skin autoimmune patterns. *Nature* (2022), doi:10.1038/s41586-021-04221-8.

24. A. Lachmann, H. Xu, J. Krishnan, S. I. Berger, A. R. Mazloom, A. Ma'ayan, ChEA: Transcription factor regulation inferred from integrating genome-wide ChIP-X experiments. *Bioinformatics* (2010), doi:10.1093/bioinformatics/btq466.

25. L. Fang, M. Zhang, Y. Li, Y. Liu, Q. Cui, N. Wang, PPARgene: A Database of Experimentally Verified and Computationally Predicted PPAR Target Genes. *PPAR Res.*

2016, 6042162 (2016).

26. P. Tontonoz, L. Nagy, J. G. A. Alvarez, V. A. Thomazy, R. M. Evans, PPARγ Promotes Monocyte/Macrophage Differentiation and Uptake of Oxidized LDL. *Cell*. **93**, 241–252 (1998).

27. M. Grabacka, W. Placha, K. Urbanska, P. Laidler, P. M. Płonka, K. Reiss, PPARγ regulates MITF and β-catenin expression and promotes a differentiated phenotype in mouse melanoma S91. *Pigment Cell Melanoma Res.* (2008), doi:10.1111/j.1755-148X.2008.00460.x.

28. D. Cipolletta, M. Feuerer, A. Li, N. Kamei, J. Lee, S. E. Shoelson, C. Benoist, D. Mathis, PPAR-γ is a major driver of the accumulation and phenotype of adipose tissue T reg cells. *Nature* (2012), doi:10.1038/nature11132.

29. C. Schuster, C. Vaculik, M. Prior, C. Fiala, M. Mildner, W. Eppel, G. Stingl, A. Elbe-Bürger, Phenotypic Characterization of Leukocytes in Prenatal Human Dermis. *J. Invest. Dermatol.* **132**, 2581–2592 (2012).

30. R. A. Spritz, G. H. L. Andersen, Genetics of Vitiligo. *Dermatol. Clin.* (2017), doi:10.1016/j.det.2016.11.013.

31. P. Bankhead, M. B. Loughrey, J. A. Fernández, Y. Dombrowski, D. G. McArt, P. D. Dunne, S. McQuaid, R. T. Gray, L. J. Murray, H. G. Coleman, J. A. James, M. Salto-Tellez, P. W. Hamilton, QuPath: Open source software for digital pathology image analysis. *Sci. Rep.* **7**, 16878 (2017).

Acknowledgments:

We gratefully acknowledge the BRC flow cytometry core at the Guy's Hospital for their assistance with flow cytometry. Genomics Centre at the Blizard Institute assisted with scRNA-seq. We also thank Dr Aamir Ahmed and Boyu Xie for assistance with tissue microarray, and imaging facility staff at University College London.

Funding:

Wellcome Trust 220009/Z/19/Z (IC)
Wellcome Trust 224910/Z/21/Z (ZJX)
Wellcome Trust 213401/Z/18/Z (NA)

Author contributions:

Conceptualization: IC, NA

Methodology: IC, NA

Investigation: IC, JX, SA

Visualization: IC

Funding acquisition: IC, NA

Project administration: NA

Supervision: NA

Writing – original draft: IC

Writing – review & editing: IC

Competing interests: Authors declare that they have no competing interests.

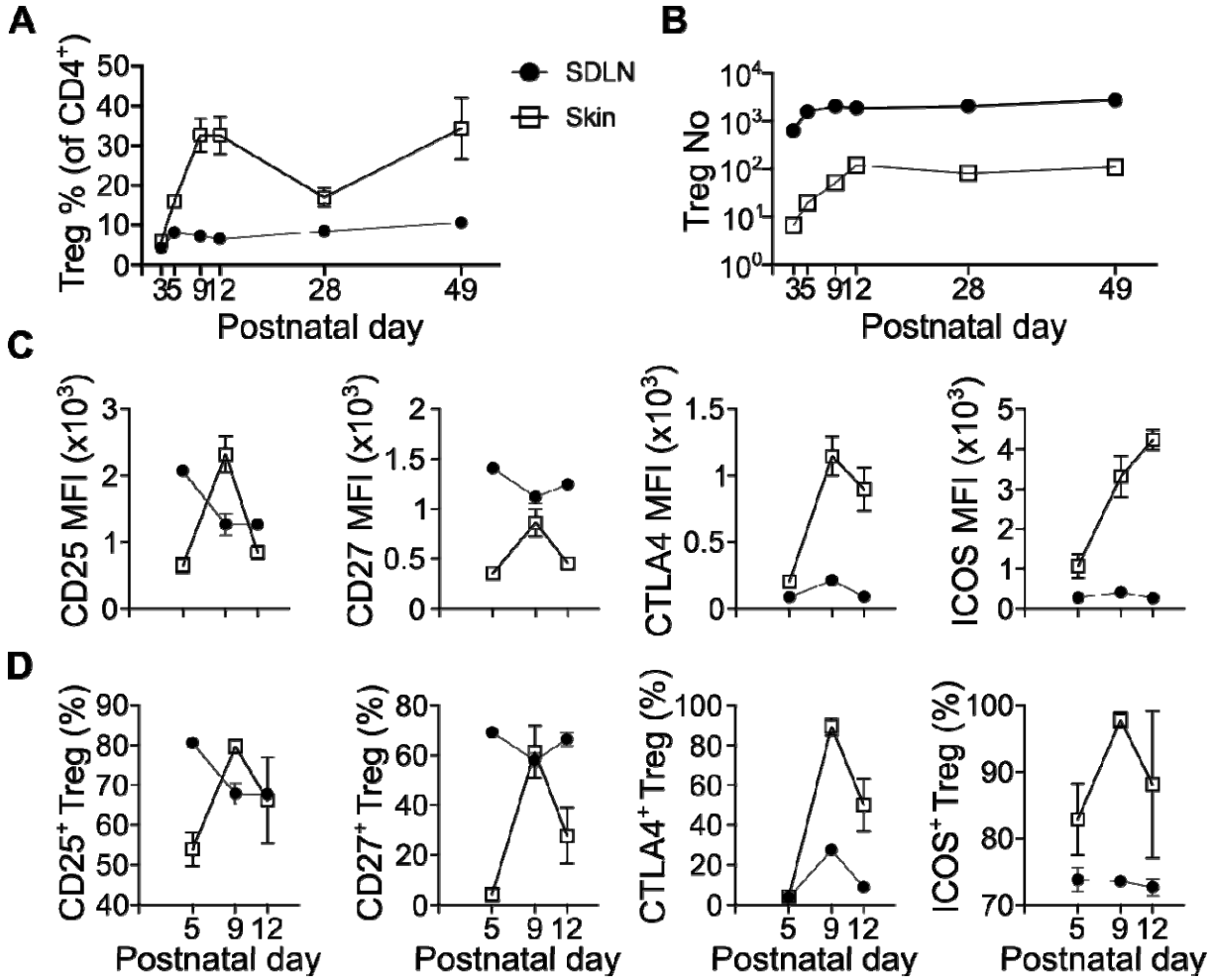

Figure 1. Neonatal skin Tregs accumulate and undergo drastic changes in phenotypic marker expression during the first two weeks of life. A-D) Flow cytometric profiling of skin $CD4^+$ $FoxP3^+$ regulatory T cells (Tregs) (n=4-6 biological replicates) pooled from 2 independent experiments. **A)** Percentage of Tregs in the skin (of total $CD4^+$ T cells) in the skin and the skin-draining lymph node (SDLN) on postnatal day 3 (P3), P5, P9, P12, P28 and P49. **B)** Absolute number of Tregs in the skin (per 6 cm^2 of skin) and SDLN (per 10^5 of total cells) on P5, P9 and P12. **C)** Median fluorescence intensities (MFIs) Treg phenotypic markers, CD25, CD27, ICOS and CTLA4. **D)** Percentage of Tregs expressing CD25, CD27, ICOS and CTLA4 (of total Tregs). Graphs show mean ± S.E.M. (n=4-6 biological replicates).

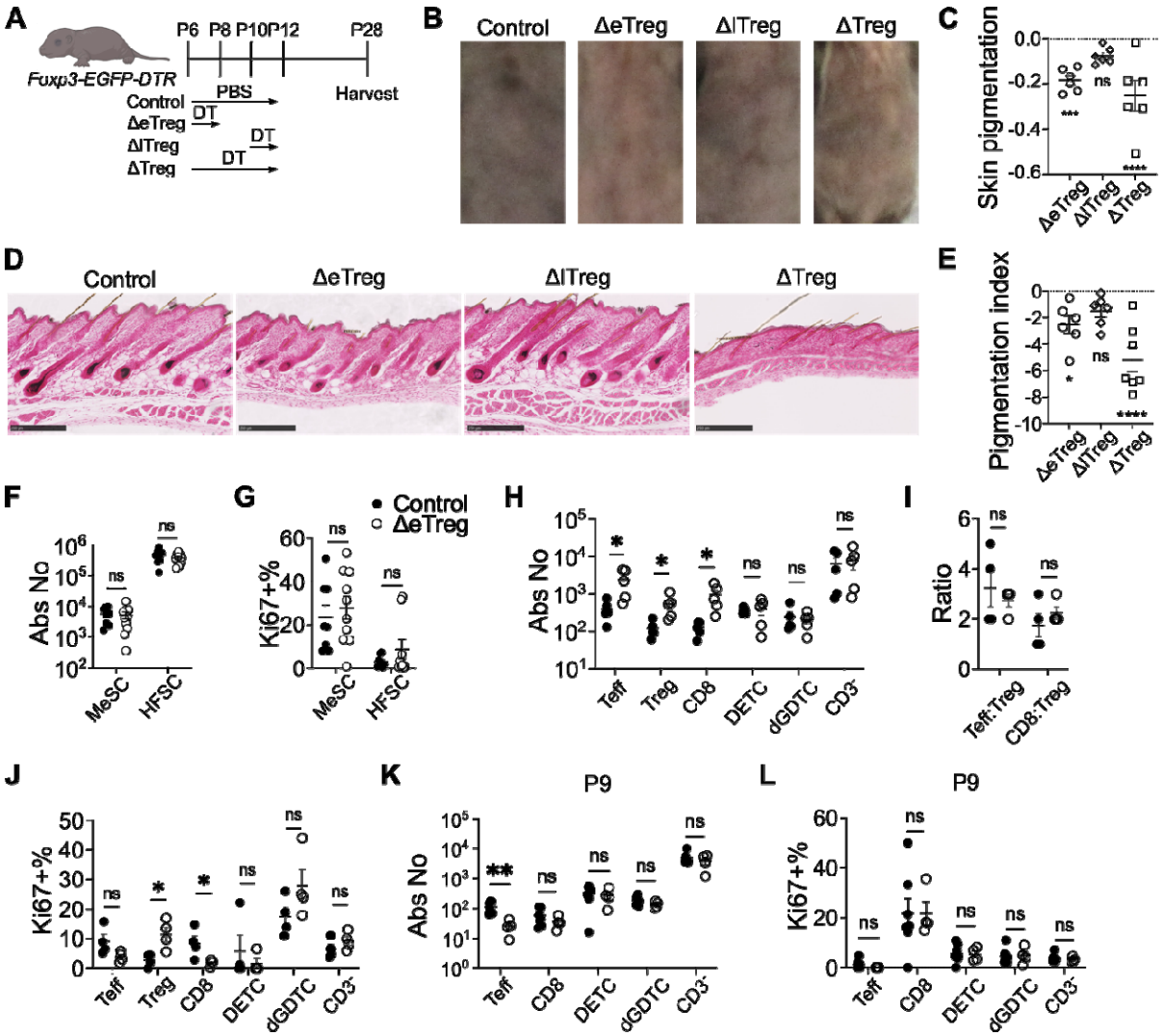

Figure 2. Early neonatal Tregs are required for skin pigmentation. A) Schematic outline of experimental timeline. *Foxp3-DTR* transgenic mice received PBS on postnatal day 6 (P6), P8, P10 and P12 (Control), DT on P6 and P8 (ΔeTreg), on P10 and P12 (ΔlTreg), and on P6, P8, P10 and P12 (ΔTreg). Skin tissues were harvested on P28. **B)** Representative Fontana & Masson staining, showing black melanin pigments. Pigmentation area was quantified and normalised against PBS control group. Scale bars represent 250 µm. **C)** Quantification of pigmentation index normalised to PBS-injected controls. **D-E)** Flow cytometric quantification of melanocyte stem cell (MeSC) and hair follicle stem cell (HFSC) **D)** Abundance and **E)** Proliferating Ki67$^+$ cells. **F-I)** Flow cytometric characterisation of the skin on P28. **F)** Absolute number of skin-resident immune cells **G)** Proliferating Ki67$^+$ immune cells. **H)** CD4$^+$ FoxP3$^-$ effector T cell (Teff):CD4$^+$ FoxP3$^+$ Treg ratio and CD8$^+$ T cell (CD8):Treg ratio. **I)** Median fluorescence intensity of Treg phenotypic markers, CD25, CD27, ICOS and CTLA4. Cells were pre-gated as CD4$^+$ FoxP3$^+$ Tregs. **J-K)** Flow cytometric characterisation of skin-resident immune cells on P9. **J**) Absolute number. **K)** Ki67$^+$ immune cells. Graphs show mean ± SEM. **B-I)** Data is representative of 4 independent experiments. **J-K)** Data is representative of two independent experiments. Unpaired t-test. ****p<0.0001, **p<0.01, *p<0.05, ns p>0.05.

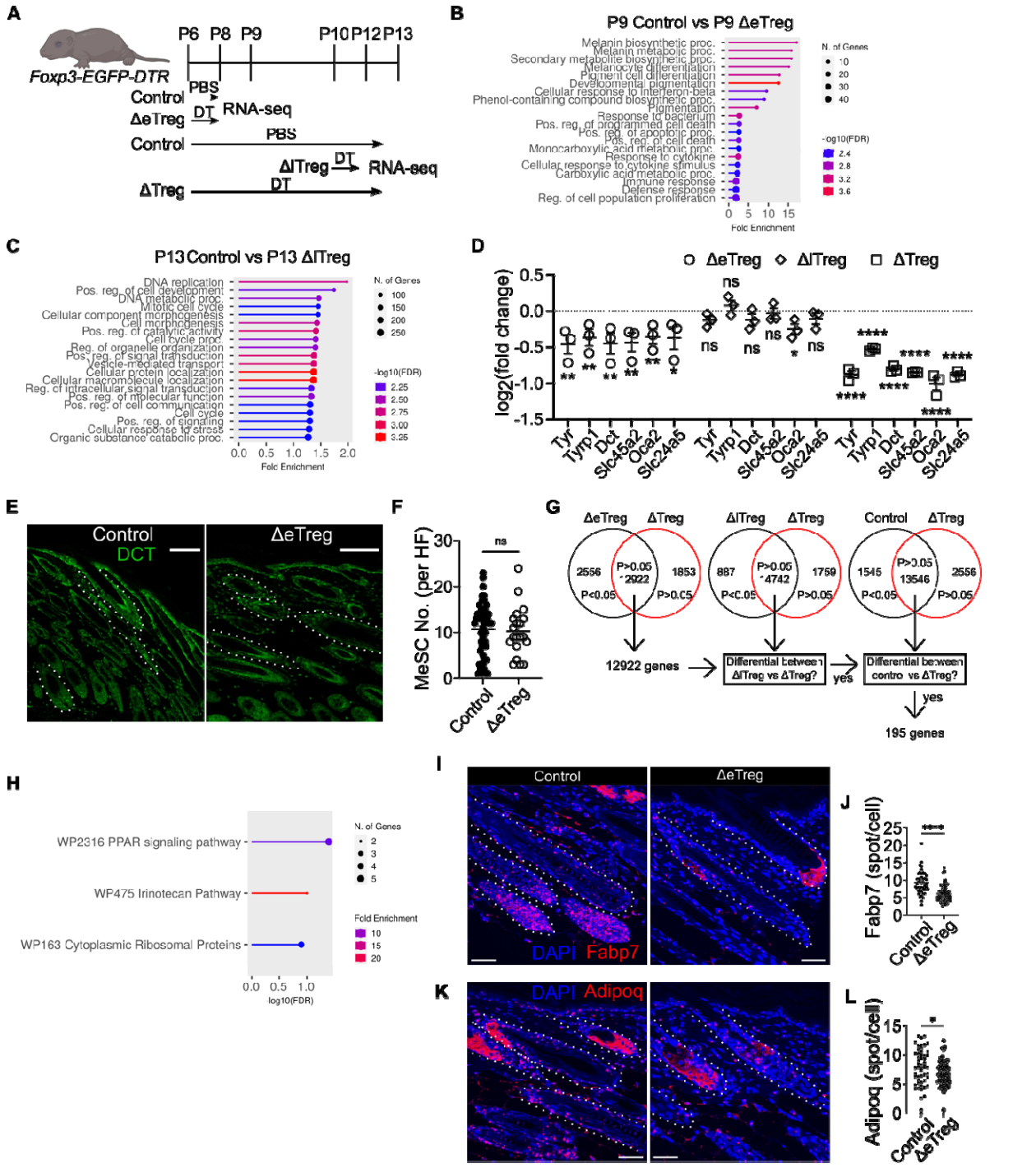

Figure 3. Melanocyte identity and PPARγ activity depend on the presence of early neonatal Tregs. A) Schematic outline of experimental timeline. Skin tissues were harvested for bulk RNA-seq on P9 or on P13 depending on treatment group. **B-C)** Enrichment analysis using differentially expressed genes ($p<0.05$) between age-matched groups. **B)** Control vs ΔeTreg skin on P9. **C)** Control vs ΔlTreg on P13. **D)** Normalised expression of melanocyte marker genes. Transcript counts were normalised to age-matched controls (n=2-3 biological replicates). **E)** Immunofluorescence staining of DCT^+ MeSCs in control and ΔeTreg dorsal skin on P9. 100 µm scale bar. **F)** Quantification of MeSC numbers per hair follicle (HF). Unpaired t-test. **G)**

Schematic outline of workflow to identify pigmentation-associated genes. 12922 Transcripts that were non-differentially expressed ($p>0.05$) between ΔeTreg and ΔTreg were sequentially filtered. Amongst 12922 transcripts, 195 were also differential ($p<0.05$) between ΔTreg and ΔlTreg, and ΔTreg and control. **H)** Pathway analysis using pigmentation-associated genes. **I-L)** RNAscope of PPARγ target genes *in situ.* P9 control and ΔeTreg skin. 50 µm scale bar. **I)** *Fabp7* and **J**) Quantification of *Fabp7* transcripts in the hair follicle (HF). **K)** *Adipoq* and **L)** Quantification of *Adipoq* transcripts in the HF. **E-L)** Data is representative of 3 independent experiments (n=3-4 biological replicates). Unpaired t-test. ****$p<0.0001$, **$p<0.01$, *$p<0.05$, ns $p>0.05$. Graphs show mean ± SEM.

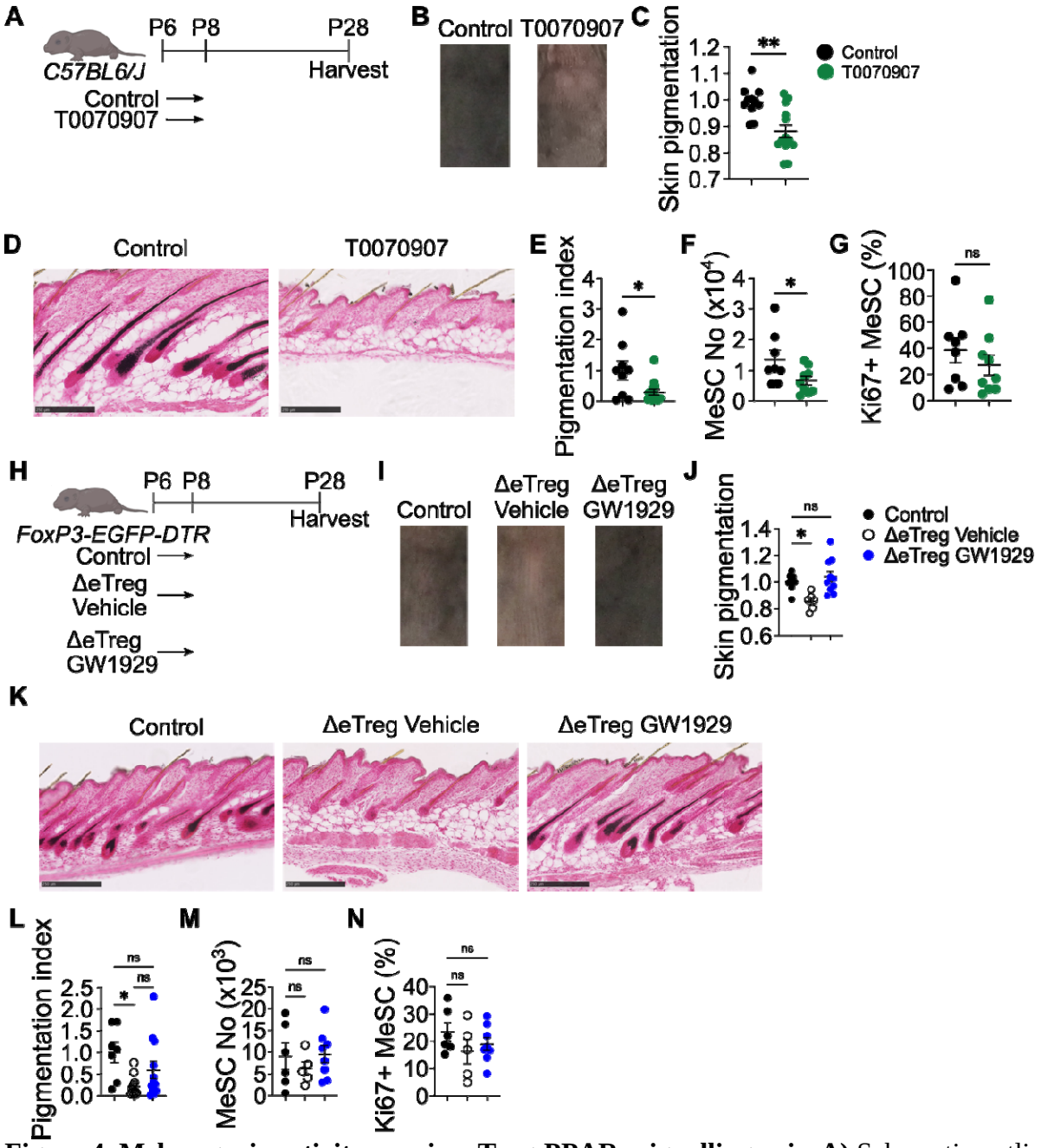

Figure 4. Melanogenic activity requires Treg-PPARγ signalling axis. A) Schematic outline of PPARγ antagonisation experiment. Control group received DMSO on P6 and P8. T0070907 group received the 2.5 µg/g of PPARγ antagonist, T0070907, on P6 and P8. **B)** Shaved dorsal skin of control and T0070907 mice. **C)** Quantification of skin pigmentation. **D)** Fontana & Masson staining. **E)** Quantification of pigmentation index. **F-G)** Flow cytometric characterisation of MeSCs. **F)** Absolute number. **G)** Percentage of Ki67^{+} MeSCs. **H)** Schematic outline of rescue experiment using PPARγ agonist. Control group received PBS and DMSO on P6 and P8. Treg-depleted ΔeTreg groups received DMSO (vehicle) or GW1929 in addition to DT on P6 and P8. Skin tissues were harvested on P28. **I)** Shaved dorsal skin. **J)** Quantification of skin pigmentation. **K)** Fontana & Masson staining. **L)** Quantification of pigmentation index. Pigmentation was normalised to control. **M-N)** Flow cytometric characterisation of MeSCs. **M)**

Absolute number. **N)** Proliferating Ki67^{+} MeSCs. **C, E-G)** Unpaired t-test. **J, L-N)** One way ANOVA against control. Graphs show mean ± SEM. Data is pooled from 2 independent experiments (n=4-6 biological replicates). ***$p<0.001$, **$p<0.01$, *$p<0.05$, ns $p>0.05$.

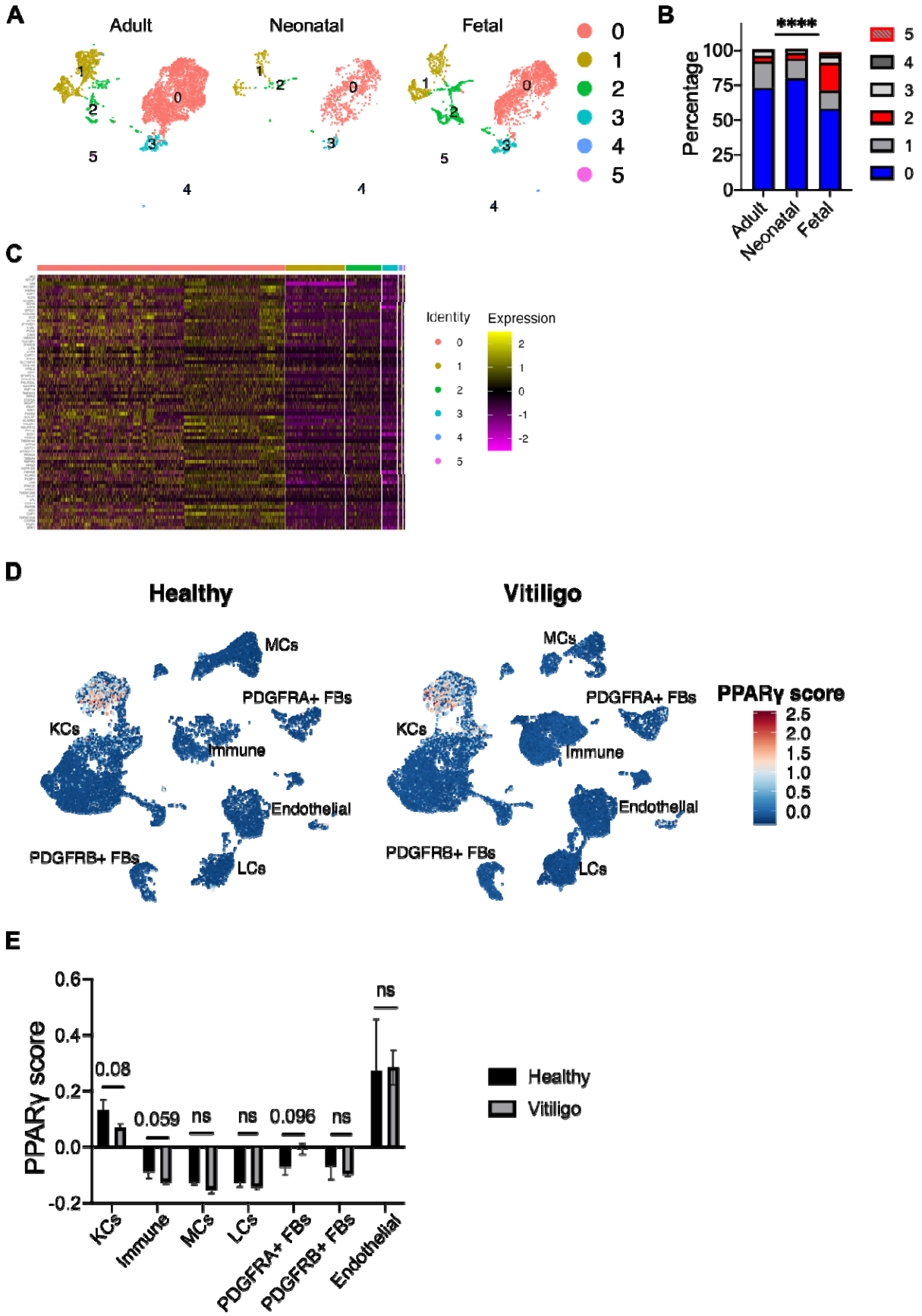
A
Adult
Neonatal
Fetal
0
1
2
3
4
5
B
****
Percentage
100
75
50
25
0
Adult
Neonatal
Fetal
C
Identity
Expression
D
Healthy
Vitiligo
MCs
PDGFRA+ FBs
KCs
Immune
Endothelial
PDGFRB+ FBs
LCs
PPARγ score
2.5
2.0
1.5
1.0
0.5
0.0
E
PPARγ score
0.6
0.4
0.2
0.0
-0.2
0.08
0.059
ns
ns
0.096
ns
ns
KCs
Immune
MCs
LCs
PDGFRA+ FBs
PDGFRB+ FBs
Endothelial
Healthy
Vitiligo

Figure 5. PPARγ target genes are differentially regulated between human developmental stages and diseased states. A-C) scRNA-seq analysis of fetal, neonatal, and adult melanocytes. **A)** UMAP representation of clusters. **B)** Percentage of cells belonging to individual clusters. Chi-squared test. **C)** Heatmap of PPARγ target gene expression. **D-E)** scRNA-seq analysis of skin from healthy donors and vitiligo patients. **D)** UMAP representation of PPARγ target gene expression score. KCs, keratinocytes. Immune, immune cells. MCs, melanocytes. LCs, Langerhans cells. PDGFRA+ FBs, PDGFRA+ fibroblasts. PDGFRB+ FBs, PDGFRB+ fibroblasts. Endothelial, endothelial cells. **E)** Quantification of PPARγ score. Unpaired t-test. ns $p>0.1$. ****$p<0.0001$.

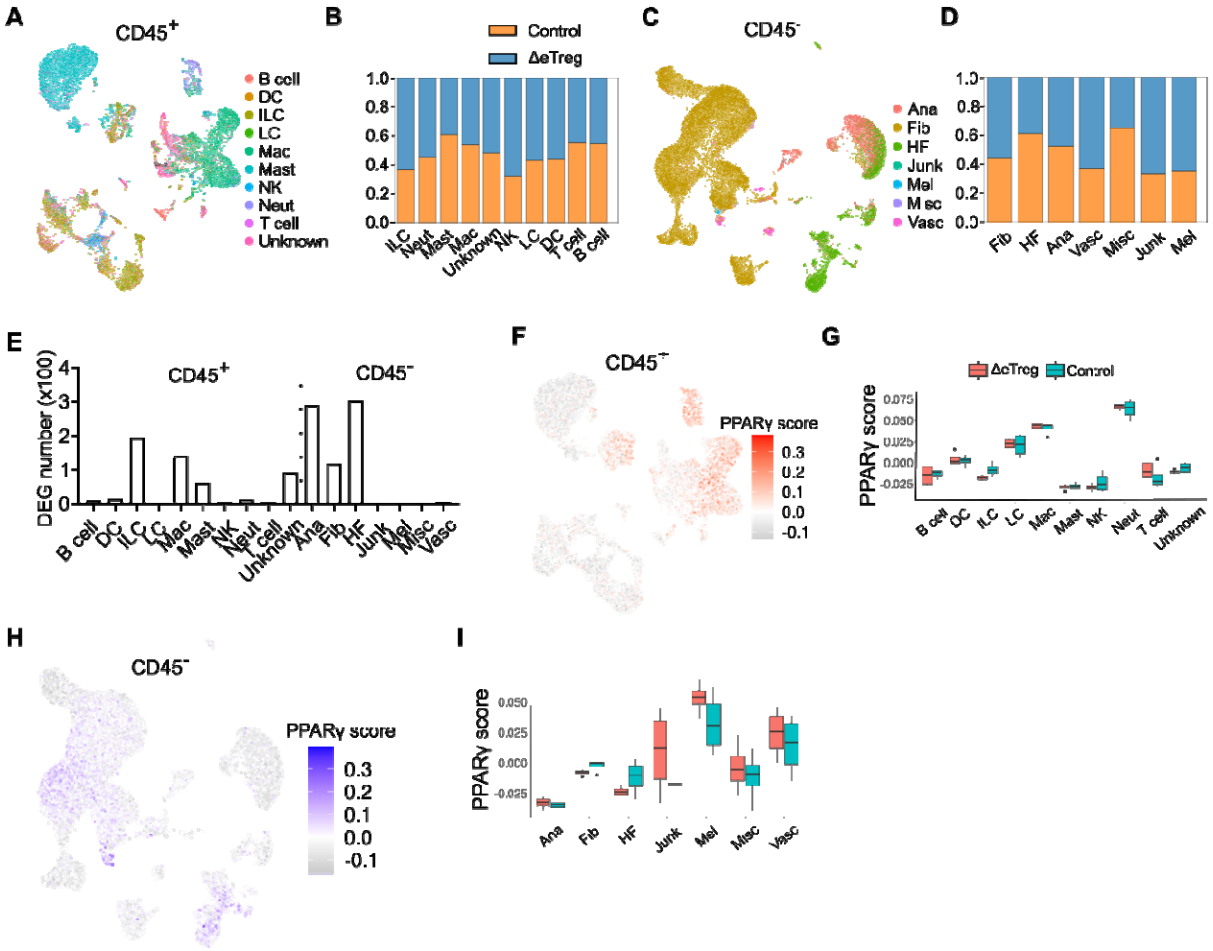

Figure 6. Neonatal Tregs regulate the hair follicle transcriptome and PPARγ activity. A) UMAP of CD45$^+$ immune cells. B cell. DC, dendritic cell. ILC, innate lymphoid cell. LC, Langerhans cell. Mac, macrophage. Mast, mast cell. NK, natural killer cell. Neut, neutrophil. T cell. Unknown. **B)** Ratio of immune cells in control and ΔeTreg skin. **C)** UMAP of CD45$^-$ non-immune cells. **D)** Ratio of non-immune cells in control and ΔeTreg skin. Ana, anagen hair follicle. Fib, fibroblast. HF, hair follicle. Junk. Mel, melanocyte. Misc, miscellaneous. Vasc, vascular cell. **E)** Number of differentially expressed genes (DEG) by cell type. **F-I)** PPARγ activity score. **F-G)** CD45$^+$ immune cells. **F)** UMAP representation. **G)** PPARγ score by cell type between control and ΔeTreg skin. **H-I)** CD45$^-$ non-immune cells. **H)** UMAP representation. **I)** PPARγ score by cell type.